DO-TH 03/09

arXiv:hep-ph/0306275v1 27 Jun 2003

Manifestly Covariant Analysis of the QED Compton Process in $ep \to e\gamma p$ and $ep \to e\gamma X$

A. Mukherjee[*] **and C. Pisano**[†]

Institut für Physik, Universität Dortmund, D 44221 Dortmund, Germany

(Dated: February 1, 2008)

Abstract

We calculate the unpolarized QED Compton scattering cross section in a manifestly covariant way. Our approach allows a direct implementation of the specific kinematical cuts imposed in the experiments, *e. g.* HERA-H1. We compare the 'exact' cross section in terms of the structure functions $F_{1,2}(x_B, Q^2)$, assuming the Callan-Gross relation, with the one obtained using the equivalent photon approximation (EPA) as well as with the experimental results. We find that the agreement with the EPA is better in x_γ bins, where x_γ is the fraction of the longitudinal momentum of the proton carried by the virtual photon, compared to the bins in the leptonic variable x_l.

---

[*] Electronic address: asmita@physik.uni-dortmund.de

[†] Electronic address: pisano@physik.uni-dortmund.de

I. INTRODUCTION

The QED Compton scattering in high energy electron-proton collisions $e(l)p(P) \rightarrow e(l')\gamma(k')X$, with a real photon $\gamma(k')$ emitted at the lepton vertex (Fig.1), is one of the most important processes for an understanding of the photon content of the proton in the so-called 'equivalent photon' approximation (EPA), first introduced for a charged particle by Weizsäcker and Williams [1] and later extended to the nucleon and investigated widely [2, 3, 4, 5, 6, 7, 8]. QED Compton scattering has been recently analyzed by the H1 collaboration at HERA [9]. In addition to the information concerning the photon content of the proton within the framework of EPA, it can also shed some light on the structure functions $F_{1,2}(x_B, Q^2)$ of the proton [9, 10] in the low-Q^2 region, which are presently poorly known [11]. In [9] these alternative descriptions were confronted with data and it was found that the description in terms of $F_{1,2}$, *i.e.* for $X \neq p$, is superior to the one in terms of the inelastic photon distribution $\gamma_{\text{inel}}(x_B, Q^2)$. Henceforth we shall refer to the description in terms of $F_{1,2}$ as 'exact' to distinguish it from the approximations involved in the EPA. It should be noted, however, that the analysis in [9, 10] utilized the Callan-Gross relation [12] $F_L(x_B, Q^2) = F_2(x_B, Q^2) - 2x_B F_1(x_B, Q^2) = 0$. This relation is contaminated by higher order (NLO) QCD corrections as well as by higher twist contributions relevant in the low-Q^2 region which may invalidate the assumptions underlying the 'exact' analysis. Furthermore, the analysis in [9, 10] was carried out within the framework of the helicity amplitude formalism [10]. The implementation of experimental cuts within this formalism is nontrivial and affords therefore an iterative numerical approximation procedure [10, 13] whose first step corresponds to $-k^2 = Q^2 = 0$, where k is the momentum of the virtual photon.

It is this second issue which we intend to study here. We shall replace the noncovariant helicity amplitude analysis of [10] by a standard covariant tensor analysis whose main advantage, besides compactness and transparency, is the possibility to implement the experimental cuts directly and thus avoid the necessity of employing an iterative approximation of limited accuracy. The first issue concerning the F_L contributions affords some estimates of this poorly known structure function and we refrain from its study here.

The plan of the paper is as follows. In section II, we calculate the exact cross section for the elastic scattering. In section III, we calculate the cross section for the inelastic channel. Our numerical results are discussed in section IV. The summary is given in section V. All the useful and necessary formulae and the kinematics are given in the appendices A, B, C and D.

II. ELASTIC QED COMPTON SCATTERING

We consider elastic QED Compton scattering:

$$e(l) + p(P) \to e(l') + \gamma(k') + p(P'), \tag{2.1}$$

where the 4-momenta of the particles are given in the brackets. We introduce the invariants

$$S = (P + l)^2, \qquad \hat{s} = (l + k)^2, \qquad t = k^2. \tag{2.2}$$

Here $k = P - P'$ is the 4-momentum of the virtual photon. The photon in the final state is real, $k'^2 = 0$. We neglect the electron mass everywhere except when it is necessary to avoid divergences in the formulae and take the proton to be massive, $P^2 = P'^2 = m^2$. The relevant Feynman diagrams for this process are shown in Fig. 1, with X being a proton and $P_X = P'$. The squared matrix element can be written as

$$\overline{\mid M_{\rm el} \mid^2} = \frac{1}{t^2} H_{\rm el}^{\mu\nu}(P, P') T_{\mu\nu}(l, k; l', k'), \tag{2.3}$$

where

$$H_{\rm el}^{\mu\nu}(P, P') = \frac{1}{2} \sum_{\rm spins} \langle P' \mid J^\nu(0) \mid P\rangle^* \langle P' \mid J^\mu(0) \mid P\rangle \tag{2.4}$$

is the hadronic tensor, J^μ being the electromagnetic current.

If we use the notation

$$dPS_N(p; p_1, ..., p_N) = (2\pi)^4 \delta(p - \sum_{i=1}^{N} p_i) \prod_{i=1}^{N} \frac{d^3 p_i}{(2\pi)^3 2p_i^0} \tag{2.5}$$

for the Lorentz invariant N-particle phase-space element, the total cross section will be

$$\sigma_{\rm el}(S) = \frac{1}{2(S - m^2)} \int dPS_{2+1}(l + P; l', k', P') \overline{\mid M_{\rm el} \mid^2} \ . \tag{2.6}$$

Eq. (2.6) can be rewritten following the technique of [2], which we slightly modify to implement the experimental cuts and constraints; in particular all the integrations are performed numerically. Rearranging the $(2 + 1)$-particle phase space into a sequence of two 2-particle ones, Eq. (2.6) becomes:

$$\sigma_{\rm el}(S) = \frac{1}{2(S - m^2)} \int \frac{d\hat{s}}{2\pi} dPS_2(l + P; l' + k', P') \frac{1}{t^2} H_{\rm el}^{\mu\nu}(P, P') X_{\mu\nu}(l, k) \ . \tag{2.7}$$

$X_{\mu\nu}$ contains all the informations about the leptonic part of the process and is defined as

$$X_{\mu\nu}(l,k) = \int dPS_2(l+k;l',k')T_{\mu\nu}(l,k;l',k'), \tag{2.8}$$

$T_{\mu\nu}$ being the leptonic tensor [14, 15]:

$$\begin{aligned} T_{\mu\nu}(l,k;l',k') = \frac{4e^4}{\hat{s}\hat{u}} \Big\{ & \frac{1}{2}\, g_{\mu\nu}\,(\hat{s}^2+\hat{u}^2+2\hat{t}t) + 2\hat{s}\, l_\mu l_\nu + 2\hat{u}\, l'_\mu l'_\nu \\ & + (\hat{t}+t)(l_\mu l'_\nu + l_\nu l'_\mu) - (\hat{s}-t)\,(l_\mu k'_\nu + l_\nu k'_\mu) \\ & + (\hat{u}-t)\,(l'_\mu k'_\nu + l'_\nu k'_\mu) \Big\}, \end{aligned} \tag{2.9}$$

where we have defined $\hat{t}=(l-l')^2$ and $\hat{u}=(l-k')^2$. It can be shown that

$$dPS_2(l+k;l',k') = \frac{d\hat{t}\, d\varphi^*}{16\,\pi^2(\hat{s}-t)}, \tag{2.10}$$

with φ^* denoting the azimuthal angle of the outgoing $e-\gamma$ system in the $e-\gamma$ c.m. frame. For unpolarized scattering, $X_{\mu\nu}$ is symmetric in the indices μ, ν and can be expressed in terms of the two Lorentz scalars $\tilde{X}_1$ and $\tilde{X}_2$:

$$\begin{aligned} X_{\mu\nu}(l,k) \; = \; \frac{1}{2t}\Big\{ & [3\tilde{X}_1(\hat{s},t)+\tilde{X}_2(\hat{s},t)]\Big(\frac{2t}{\hat{s}-t}l-k\Big)_\mu\Big(\frac{2t}{\hat{s}-t}l-k\Big)_\nu \\ & + [\tilde{X}_1(\hat{s},t)+\tilde{X}_2(\hat{s},t)](tg_{\mu\nu}-k_\mu k_\nu)\Big\}, \end{aligned} \tag{2.11}$$

with

$$\tilde{X}_1(\hat{s},t) = \frac{4t}{(\hat{s}-t)^2} l^\mu l^\nu X_{\mu\nu}(l,k), \tag{2.12}$$

$$\tilde{X}_2(\hat{s},t) = g^{\mu\nu}X_{\mu\nu}(l,k). \tag{2.13}$$

Using the leptonic tensor (2.9) and also the relations

$$l\cdot k = \frac{1}{2}(\hat{s}-t), \quad\; l\cdot P = \frac{1}{2}(S-m^2), \quad k\cdot P = \frac{1}{2}t, \tag{2.14}$$

we obtain

$$\frac{t\, l^\mu l^\nu T_{\mu\nu}}{4\pi^2(\hat{s}-t)^3} = e^4\, \frac{-t\hat{t}}{2\pi^2(\hat{s}-t)^3} \equiv X_1(\hat{s},t,\hat{t}), \tag{2.15}$$

$$\frac{g^{\mu\nu}T_{\mu\nu}}{16\pi^2(\hat{s}-t)} = e^4\, \frac{(t^2-2t\hat{s}+2\hat{s}^2+2\hat{s}\hat{t}+\hat{t}^2)}{4\pi^2\hat{s}(\hat{s}-t)(t-\hat{s}-\hat{t})} \equiv X_2(\hat{s},t,\hat{t}), \tag{2.16}$$

where $e^2 = 4\pi\alpha$. The invariants $X_i(\hat{s}, t, \hat{t})$, with $i = 1, 2$, are related to $\tilde{X}_i(\hat{s}, t)$ by

$$\tilde{X}_i(\hat{s}, t) = 2\pi \int_{\hat{t}_{\min}}^{\hat{t}_{\max}} d\hat{t}\, X_i(\hat{s}, t, \hat{t}). \tag{2.17}$$

The integration limits of $\hat{t}$ are:

$$\hat{t}_{\max} = 0, \qquad \hat{t}_{\min} = -\hat{s} + t + \frac{\hat{s}}{\hat{s} - t}\, m_e^2, \tag{2.18}$$

where m_e is the mass of the electron. We point out that the kinematical cuts employed by us prevent the electron propagators to become too small and thus the divergences are avoided, so we can safely neglect the electron mass in the numerial calculation. The hadronic tensor in the case of elastic scattering can be expressed in terms of the common proton form factors as

$$H_{\rm el}^{\mu\nu}(P, P') = e^2 \left[H_1(t)(2P - k)^\mu (2P - k)^\nu + H_2(t)(t g^{\mu\nu} - k^\mu k^\nu)\right], \tag{2.19}$$

with

$$H_1(t) = \frac{G_E^2(t) - (t/4\,m^2)\, G_M^2(t)}{1 - t/4\,m^2}, \qquad H_2(t) = G_M^2(t). \tag{2.20}$$

The electric and magnetic form factors are empirically parametrized as dipoles:

$$G_E(t) = \frac{1}{[1 - t/(0.71\,\mathrm{GeV}^2)]^2}, \qquad G_M(t) = 2.79\; G_E(t). \tag{2.21}$$

Using

$$dPS_2(l + P; l' + k', P') = \frac{dt}{8\pi(S - m^2)}, \tag{2.22}$$

finally we get

$$\begin{aligned}\sigma_{\rm el}(S) \;=\; & \frac{\alpha}{8\pi(S - m^2)^2} \int_{\hat{s}_{\min}}^{(\sqrt{S}-m)^2} d\hat{s} \int_{t_{\min}}^{t_{\max}} \frac{dt}{t} \int_{\hat{t}_{\min}}^{\hat{t}_{\max}} d\hat{t} \int_0^{2\pi} d\varphi^* \bigg\{ \bigg[2\, \frac{S - m^2}{\hat{s} - t} \bigg(\frac{S - m^2}{\hat{s} - t} - 1 \bigg) \\ & \times [3X_1(\hat{s}, t, \hat{t}) + X_2(\hat{s}, t, \hat{t})] + \frac{2m^2}{t} [X_1(\hat{s}, t, \hat{t}) + X_2(\hat{s}, t, \hat{t})] + X_1(\hat{s}, t, \hat{t}) \bigg] H_1(t) \\ & + X_2(\hat{s}, t, \hat{t}) H_2(t) \bigg\},\end{aligned} \tag{2.23}$$

where $\hat{s}_{\min}$ denotes the minimum of $\hat{s}$ and $t_{\min,\,\max}$ are given by

$$t_{\min,\,\max} = 2m^2 - \frac{1}{2S}\Big[(S + m^2)(S - \hat{s} + m^2) \pm (S - m^2)\sqrt{(S - \hat{s} + m^2)^2 - 4Sm^2}\,\Big]. \tag{2.24}$$

It is to be noted that in Eq. (2.23) we have shown the integration over φ^* explicitly, because of the cuts that we shall impose on the integration variables for the numerical calculation of the cross section. The cuts are discussed in section IV. The EPA consists of considering the exchanged photon as real, so it is particularly good for the elastic process in which the virtuality of the photon $|t|$ is constrained to be small ($\lesssim 1\,\mathrm{GeV}^2$) by the form factors. It is possible to get the approximated cross section $\sigma_{\rm el}^{\rm EPA}$ from the exact one in a straightforward way, following again [2]. If the invariant mass of the system $e-\gamma$ is large compared to the proton mass, $\hat{s}_{\rm min} \gg m^2$, one can neglect $|t|$ versus $\hat{s}$, m^2 versus S, then

$$X_1(\hat{s}, t, \hat{t}) \approx X_1(\hat{s}, 0, \hat{t}) = 0, \tag{2.25}$$

and

$$X_2(\hat{s}, t, \hat{t}) \approx X_2(\hat{s}, 0, \hat{t}) = -\frac{2\hat{s}}{\pi}\,\frac{d\hat{\sigma}(\hat{s}, \hat{t})}{d\hat{t}}, \tag{2.26}$$

where we have introduced the differential cross-section for the real photoproduction process $e\gamma \to e\gamma$:

$$\frac{d\hat{\sigma}(\hat{s}, \hat{t})}{d\hat{t}} = -\frac{2\pi\alpha^2}{\hat{s}^2}\left(\frac{\hat{u}}{\hat{s}} + \frac{\hat{s}}{\hat{u}}\right), \tag{2.27}$$

with $\hat{u} = -\hat{s} - \hat{t}$. We get:

$$\sigma_{\rm el}(S) \approx \sigma_{\rm el}^{\rm EPA} = \int_{x_{\rm min}}^{(1-m/\sqrt{S})^2} dx \int_{m_e^2-\hat{s}}^{0} d\hat{t}\,\gamma_{\rm el}(x)\,\frac{d\hat{\sigma}(xS, \hat{t})}{d\hat{t}}, \tag{2.28}$$

where $x = \hat{s}/S$ and $\gamma_{\rm el}(x)$ is the elastic contribution to the equivalent photon distribution of the proton [2, 7]:

$$\gamma_{\rm el}(x) = -\frac{\alpha}{2\pi}x\int_{t_{\rm min}}^{t_{\rm max}} \frac{dt}{t}\left\{2\left[\frac{1}{x}\left(\frac{1}{x} - 1\right) + \frac{m^2}{t}\right]H_1(t) + H_2(t)\right\}, \tag{2.29}$$

with

$$t_{\rm min} \approx -\infty \qquad\qquad t_{\rm max} \approx -\frac{m^2x^2}{1-x}. \tag{2.30}$$

To clarify the physical meaning of x, let us introduce the variable x_γ:

$$x_\gamma = \frac{l\cdot k}{P\cdot l}. \tag{2.31}$$

It is possible to show that x_γ represents the fraction of the longitudinal momentum of the proton carried by the virtual photon, so that one can write

$$k = x_\gamma P + \hat{k}, \tag{2.32}$$

with $\hat{k} \cdot P = 0$. Using (2.2) one gets

$$x_\gamma = \frac{\hat{s} - t}{S - m^2}, \tag{2.33}$$

which reduces to x in the EPA limit. One can also define the leptonic variable x_l:

$$x_l = \frac{Q_l^2}{2P \cdot (l - l')}, \tag{2.34}$$

where $Q_l^2 = -\hat{t}$. When $t \simeq 0$, it turns out that also $x_l \simeq x$.

III. INELASTIC QED COMPTON SCATTERING

To calculate the inelastic QED Compton scattering cross section, we extend the approach discussed in the previous section. In this case, an electron and a photon are produced in the final state with a general hadronic system X. In other words, we consider the process

$$e(l) + p(P) \rightarrow e(l') + \gamma(k') + X(P_X), \tag{3.1}$$

where $P_X = \sum_{X_i} P_{X_i}$ is the sum over all momenta of the produced hadronic system. Let the invariant mass of the produced hadronic state X to be W. Eq. (2.2) still holds with $Q^2 = -t$. The cross section for inelastic scattering will be

$$\sigma_{\rm inel}(S) = \frac{1}{2(S - m^2)} \int dPS_{2+N}(l + P; l', k', P_{X_1}, ..., P_{X_N}) \overline{\mid M_{\rm inel} \mid^2}, \tag{3.2}$$

where

$$\overline{\mid M_{\rm inel} \mid^2} = \frac{1}{Q^4} H^{\mu\nu}_{\rm inel}(P, P_X) T_{\mu\nu}(l, k; l', k') \tag{3.3}$$

is the squared matrix element and

$$H^{\mu\nu}_{\rm inel}(P, P_X) = \frac{1}{2} \sum_{\rm spins} \sum_X \langle P_X \mid J^\nu(0) \mid P \rangle^* \langle P_X \mid J^\mu(0) \mid P \rangle \ . \tag{3.4}$$

If we rearrange the $(2 + N)$-particle space phase into a sequence of a 2-particle and a N-particle one, we get

$$\sigma_{\rm inel}(S) = \frac{1}{2(S - m^2)} \int \frac{dW^2}{2\pi} \int \frac{d\hat{s}}{2\pi} \int dPS_2(l + P; l' + k', P_X) \frac{1}{Q^4} W^{\mu\nu}(P, k) X_{\mu\nu}(l, k), \tag{3.5}$$

where $X_{\mu\nu}$ is given by Eq. (2.11) and $W^{\mu\nu}$ is the hadronic tensor for inelastic scattering

$$W^{\mu\nu} = \int dPS_N(P-k; P_{X_1}, ..., P_{X_N})\, H^{\mu\nu}_{\rm inel}\ . \tag{3.6}$$

The hadronic tensor is parametrized as

$$W^{\mu\nu} = \frac{4\pi e^2}{Q^2}\Big[-(Q^2 g^{\mu\nu} + k^\mu k^\nu) F_1(x_B, Q^2) + (2x_B P^\mu - k^\mu)(2x_B P^\nu - k^\nu)\frac{F_2(x_B, Q^2)}{2x_B}\Big], \tag{3.7}$$

where x_B is the Bjorken variable given by

$$x_B = -\frac{Q^2}{2P\cdot k} = \frac{Q^2}{Q^2 + W^2 - m^2}. \tag{3.8}$$

Using

$$dPS_2(l+P; l'+k', P_X) = \frac{dQ^2}{8\pi(S-m^2)} \tag{3.9}$$

as before, we get

$$\begin{aligned}
\sigma_{\rm inel}(S) \ = \ & \frac{\alpha}{4\pi(S-m^2)^2}\int_{W^2_{\rm min}}^{W^2_{\rm max}} dW^2 \int_{\hat{s}_{\rm min}}^{(\sqrt{S}-W)^2} d\hat{s} \int_{Q^2_{\rm min}}^{Q^2_{\rm max}} \frac{dQ^2}{Q^4} \int_{\hat{t}_{\rm min}}^{\hat{t}_{max}} d\hat{t} \int_0^{2\pi} d\varphi^* \Big\{ \Big[\Big(2\,\frac{S-m^2}{\hat{s}+Q^2} \\
& \times \Big(1 - \frac{S-m^2}{\hat{s}+Q^2}\Big) + (W^2-m^2)\Big(\frac{2\,(S-m^2)}{Q^2(\hat{s}+Q^2)} - \frac{1}{Q^2} + \frac{m^2-W^2}{2\,Q^4}\Big)\Big) \\
& \times [3X_1(\hat{s},Q^2,\hat{t}) + X_2(\hat{s},Q^2,\hat{t})] + \Big(\frac{1}{Q^2}(W^2-m^2) + \frac{(W^2-m^2)^2}{2\,Q^4} + \frac{2m^2}{Q^2}\Big) \\
& \times [X_1(\hat{s},Q^2,\hat{t}) + X_2(\hat{s},Q^2,\hat{t})] - X_1(\hat{s},Q^2,\hat{t})\Big] F_2(x_B,Q^2)\frac{x_B}{2} \\
& - X_2(\hat{s},Q^2,\hat{t}) F_1(x_B,Q^2)\Big\}.
\end{aligned} \tag{3.10}$$

Here $X_i(\hat{s}, Q^2, \hat{t})$, with $i = 1, 2$, are given by Eqs. (2.15)-(2.16) with t replaced by $-Q^2$. The limits of the integration over Q^2 are:

$$Q^2_{\rm min,max} = -m^2 - W^2 + \frac{1}{2S}\Big[(S+m^2)(S-\hat{s}+W^2) \mp (S-m^2)\sqrt{(S-\hat{s}+W^2)^2 - 4SW^2}\Big], \tag{3.11}$$

while the extrema of $\hat{t}$ are the same as Eq. (2.18). The limits $W^2_{\rm min,max}$ are given by:

$$W^2_{\rm min} = (m+m_\pi)^2, \qquad W^2_{\rm max} = (\sqrt{S} - \sqrt{\hat{s}_{\rm min}}\,)^2, \tag{3.12}$$

where m_π is the mass of the pion. F_1 and F_2 are the usual structure functions of the proton.

In the EPA, we neglect m^2 compared to S and Q^2 compared to $\hat{s}$ as before. Using Eqs. (2.25) and (2.26), we can write

$$\sigma_{\text{inel}}(S) \approx \sigma_{\text{inel}}^{\text{EPA}} = \int_{x_{\min}}^{(1-m/\sqrt{S})^2} dx \int_{m_e^2-\hat{s}}^{0} d\hat{t}\; \gamma_{\text{inel}}(x, xS)\, \frac{d\hat{\sigma}(xS,\hat{t})}{d\hat{t}}, \tag{3.13}$$

where again $x = \hat{s}/S$ and $\gamma_{\text{inel}}(x, xS)$ is the inelastic contribution to the equivalent photon distribution of the proton [17]:

$$\begin{aligned} \gamma_{\text{inel}}(x, xS) \;=\; \frac{\alpha}{2\pi}\int_x^1 dy \int_{Q^2_{\min}}^{Q^2_{\max}} \frac{dQ^2}{Q^2}\,\frac{y}{x}\Big[F_2\Big(\frac{x}{y},Q^2\Big)\Big(\frac{1+(1-y)^2}{y^2} - \frac{2m^2x^2}{y^2Q^2}\Big) \\ - F_L\Big(\frac{x}{y},Q^2\Big)\Big]. \end{aligned} \tag{3.14}$$

Following [9, 10] we shall use the LO Callan-Gross relation

$$F_L(x_B, Q^2) \;=\; F_2(x_B, Q^2) - 2x_B F_1(x_B, Q^2) \;=\; 0 \tag{3.15}$$

in our numerical calculations. The limits of the Q^2 integration can be approximated as

$$Q^2_{\min} = \frac{x^2m^2}{1-x}, \qquad Q^2_{\max} = \hat{s}. \tag{3.16}$$

Our expression of $\gamma_{\text{inel}}(x, xS)$ differs from [11] by a (negligible) term proportional to m^2.

IV. NUMERICAL RESULTS

In this section, we present an estimate of the cross section, calculated both exactly and using the equivalent photon approximation of the proton. We have used the same kinematical cuts as used by the H1 collaboration at HERA [9], which are slightly different from the ones in [10]. They are imposed on the following lab frame variables: energy of the final electron E'_e, energy of the final photon E'_γ, polar angles of the outgoing electron and photon, θ_e and θ_γ respectively, and acoplanarity angle ϕ, which is defined as $\phi = |\,\pi - |\phi_\gamma - \phi_e|\,|$, where ϕ_γ and ϕ_e are the azimuthal angles of the outgoing photon and electron respectively ($0 \le \phi_\gamma,\ \phi_e \le 2\,\pi$). The cuts are given by:

$$E'_e, E'_\gamma > 4\,\text{GeV}, \qquad E'_e + E'_\gamma > 20\,\text{GeV}, \tag{4.1}$$

$$0.06 < \theta_e, \theta_\gamma < \pi - 0.06, \tag{4.2}$$

$$0 < \phi < \frac{\pi}{4}. \qquad (4.3)$$

The energies of the incoming particles are: $E_e = 27.5$ GeV (electron) and $E_p = 820$ GeV (proton). In our conventions, we fix the lab frame such that $\phi_e = 0$, so the acoplanarity will be $\phi = |\,\pi - \phi_\gamma\,|$. These cuts reflect experimental acceptance constraints as well as the reduction of the background events due to emitted photons with $(l' + k')^2 \approx 0$ and/or $(l - k')^2 \approx 0$, which are unrelated to the QED Compton scattering process (for which $-k^2 = Q^2 \approx 0$ but with both $(l' + k')^2$ and $(l - k')^2$ finite), *i.e.* photons emitted parallel to the ingoing (outgoing) electron or from the hadron vertex [10, 11].

We numerically integrate the elastic and inelastic cross sections given by Eqs. (2.23) and (3.10). To implement the cuts in Eqs. (4.1)-(4.3), we express E_e', E_γ', $\cos\theta_e$, $\cos\theta_\gamma$ and $\cos\phi$ in terms of our integration variables $\hat{s}$, t, $\hat{t}$, φ^* (and W^2 in the inelastic channel), as explained in Appendices A-D. More explicitly, we use Eqs. (B7)-(B11), (A7), (A8), together with Eqs. (A11)-(A13) for the elastic channel and Eqs. (C3)-(C5) for the inelastic one. The cuts imposed on the lab frame variables restrict the range of our integrations numerically. In this way, we are able to remove the contributions from outside the considered kinematical region.

In the calculation of the inelastic cross section, we have used the ALLM97 parametrization of $F_2(x_B, Q^2)$ [16], which is obtained by fitting DIS data of HERA and fixed target experiments together with the total pp and γp cross sections measured and is expected to hold over the entire available range of x_B and Q^2. We have not considered the resonance contribution separately but, using the so called local duality [6], we have extended the ALLM97 parametrization of F_2 from the continuous ($W > 1.8$ GeV) down to the resonance domain ($m + m_\pi < W < 1.8$ GeV). In this way it is possible to agree with the experimental data averaged over each resonance, as pointed out in [9]. The elastic contribution to the EPA was calculated using Eq.(2.28) subject to the additional kinematical restrictions given by Eqs. (4.1-4.2). It corresponds to the same equivalent photon distribution as presented in [6, 7, 8]. For the inelastic channel we have used Eq. (3.13) together with Eq. (3.14), the cuts being the same as in the elastic case. We have taken $F_L = 0$ and used the ALLM parametrization of F_2, in order to compare consistently with the 'exact' cross section. We point out that in [6, 7, 8], $F_2(x_B, Q^2)$ in $\gamma_{\rm inel}(x, xS)$ was expressed in terms of parton distributions for which the LO GRV parametrization [18] was used, together with $Q^2_{\rm min} = 0.26$ GeV^2 so as to guarantee the applicability of perturbative QCD [5]. $\gamma_{\rm inel}(x, xS)$ in our case gives slightly higher results than the ones obtained with the photon distribution presented in [6, 7, 8].

The Compton process turns out to be dominated by the elastic channel, in fact after Monte Carlo integration, we find that $\sigma_{\rm el} = 1.7346$ pb, while $\sigma_{\rm inel} = 1.1719$ pb. The approximated calculation gives the results: $\sigma_{\rm el}^{\rm EPA} = 1.7296$ pb and $\sigma_{\rm inel}^{\rm EPA} = 1.5969$ pb. This means that in the kinematical region under consideration, the total (elastic + inelastic) cross section calculated using the EPA agrees with the exact one within 14% and that the approximation turns out to be particularly good in describing the elastic process, for which the agreement is within 0.3%. This is not surprising since in the EPA one assumes $Q^2 = 0$, which is not true especially in the inelastic channel and the inelastic cross section receives substantial contribution from the non-zero Q^2 region. In terms of the kinematical cuts, the EPA corresponds to the situation when the outgoing electron and the final photon are observed under large polar angles and almost opposite to each other in azimuth, so that the acoplanarity is approximately zero. For elastic scattering there is a sharp peak of the exact cross section for $\phi = 0$, contributions from non-zero ϕ are very small in this case. But the inelastic cross section receives contribution even from non-zero ϕ, so that in this case the discrepancy from the approximated result is higher. The discrepancy of the total cross section with the approximate one is thus entirely due to the inelastic part.

In Fig. 2 we have compared the total cross sections (exact and EPA) in different x_l bins, in the region $1.78 \times 10^{-5} < x_l < 1.78 \times 10^{-1}$. Fig. 3 shows that the agreement improves slightly for bins in the variable x_γ. Since $x_\gamma \simeq x_l$ for $Q^2 \simeq 0$, the elastic process is not sensitive to this change of variables. We point out again that in the EPA limit ($Q^2 = 0$) $x_l = x_\gamma \equiv x$.

In Fig. 4 we show the exact and the EPA cross section in x_l and Q_l^2 bins together with the experimental results and the estimates of the Compton event generator, already presented in [9]. Except for three bins, our exact result agrees with the experiment within the error bars. The slight difference of our exact result and the one of [9] may be due to the fact that in [9] the cross section is calculated using a Monte Carlo generator in a step by step iteration [10, 13] which starts by assuming $Q^2 = 0$, while we did not use any approximation. Our exact result is closer to the EPA in most of the kinematical bins as compared to [9]. The total cross section in the EPA lies above the 'exact' one in most of the bins.

For completeness, we have shown the numerical values of the exact and EPA double differential cross sections, both for the elastic (Table 1) and inelastic (Table 2) contributions. The kinematical bins are the same as in [9]. The exact results when the bins are in x_γ instead of x_l are also shown. The EPA elastic cross section agrees within 1% with the exact one for all the x_l bins. The agreement becomes slightly better if we consider x_γ bins. For the inelastic channel, the discrepancies from the EPA results are considerably higher. Our 'exact' results lie closer to the EPA compared to [9] in almost all the bins. The result in x_γ bins show better agreement with the EPA compared to the x_l bins, especially for higher x_γ. The discrepancy with the EPA is about $20-30\%$ in most of the bins, higher in some cases.

V. SUMMARY

In this work, we have calculated both elastic and inelastic QED Compton scattering cross section in the unpolarized case. Our approach for the total cross section is manifestly covariant and we have used the same cuts as in the HERA-H1 experiment. The numerical estimates of the exact cross section for different kinematical bins are presented and compared with the EPA and the experimental results. The exact cross section in the elastic channel agrees within 1% with the approximate one. The discrepancy is thus due to the inelastic channel. The discrepancy with the Monte Carlo estimate of [9] is also shown. For both elastic and inelastic cross sections, our exact result is closer to the EPA as compared to [9]. The agreement is even better if the bins are in x_γ instead of x_l. Our approach can be extended to calculate the corresponding cross section for polarized scattering and also for other polarized and unpolarized processes having photon induced subprocesses, in order to check how accurately the cross section is given by the equivalent photon approximation. Also this would predict the kinematical cuts necessary for the extraction of $\gamma(x, Q^2)$ experimentally from these processes.

VI. ACKNOWLEDGEMENTS

We warmly acknowledge M. Glück and E. Reya for initiating this study, as well as for many helpful discussions and suggestions. We also thank V. Lendermann, M. Stratmann and I. Schienbein for helpful discussions and comments. This work has been supported in part by the 'Bundesministerium für Bildung und Forschung', Berlin/Bonn.

APPENDIX A: KINEMATICS IN THE $e-\gamma$ C. M. FRAME (ELASTIC)

In this appendix, we discuss the kinematics of the QED Compton scattering in the c. m. frame of the outgoing $e-\gamma$ system. The 4-momenta of the particles are given by:
incident electron: $l \equiv (E_e^*,\, 0,\, 0,\, -E_e^*)$,
incident proton: $P \equiv (E_p^*,\, P_p^* \sin\theta_p^*,\, 0,\, P_p^* \cos\theta_p^*)$, where $P_p^* = \sqrt{E_p^{*2} - m^2}$,
outgoing electron: $l' \equiv E'^*(1,\, \sin\theta^* \cos\varphi^*,\, \sin\theta^* \sin\varphi^*,\, \cos\theta^*)$,
outgoing photon: $k' \equiv E'^*(1,\, -\sin\theta^* \cos\varphi^*,\, -\sin\theta^* \sin\varphi^*,\, -\cos\theta^*)$.
We have also: 4-momentum of the virtual photon: $k = (E_k^*,\, 0,\, 0,\, E_e^*)$, with $k^2 = t$ and

$$E_k^* = \sqrt{E_e^{*2} + t}. \tag{A1}$$

The overall momentum conservation allows us to write the 4-momentum of the final proton as

$$P' = l + P - l' - k'. \tag{A2}$$

We introduce the following Lorentz invariants

$$\hat{s} = (l' + k')^2 = 4E'^{*2}, \tag{A3}$$

$$\hat{t} = (l - l')^2 = -2E_e^* E'^* (1 + \cos\theta^*), \tag{A4}$$

$$\hat{u} = (l - k')^2 = -2E_e^* E'^* (1 - \cos\theta^*), \tag{A5}$$

$$S = (l + P)^2 = m^2 + 2E_p^* E_e^* + 2E_e^* P_p^* \cos\theta_p^*, \tag{A6}$$

$$T = (P - l')^2 = m^2 - 2E'^* (E_p^* - P_p^* \sin\theta^* \sin\theta_p^* \cos\varphi^* - P_p^* \cos\theta^* \cos\theta_p^*), \tag{A7}$$

$$U = (P - k')^2 = m^2 - 2E'^* (E_p^* + P_p^* \sin\theta^* \sin\theta_p^* \cos\varphi^* + P_p^* \cos\theta^* \cos\theta_p^*). \tag{A8}$$

In addition they satisfy:

$$\hat{s} + \hat{t} + \hat{u} = t, \qquad S + T + U = -t + 3m^2. \tag{A9}$$

Using the relations above, it is possible to write the energies of the particles in the lab frame in terms of the integration variables $\hat{s}$, $\hat{t}$, t and the constant S:

$$E_e^* = \frac{\hat{s} - t}{2\sqrt{\hat{s}}}, \qquad E_k^* = \frac{\hat{s} + t}{2\sqrt{\hat{s}}}, \tag{A10}$$

and

$$E_p^* = \frac{S - m^2 + t}{2\sqrt{\hat{s}}}, \qquad P_p^* = \frac{\sqrt{(S - m^2 + t)^2 - 4\hat{s}m^2}}{2\sqrt{\hat{s}}}, \qquad E'^* = \frac{\sqrt{\hat{s}}}{2}. \tag{A11}$$

Similarly, for the angles we have

$$\cos\theta^* = \frac{t - \hat{s} - 2\hat{t}}{\hat{s} - t}, \tag{A12}$$

$$\cos\theta_p^* = \frac{2\hat{s}\,(S - m^2) - (\hat{s} - t)(S - m^2 + t)}{(S - t)[(S + t - m^2)^2 - 4\hat{s}m^2]^{\frac{1}{2}}}. \tag{A13}$$

In particular Eqs. (A7) and (A8), through Eqs. (A11)-(A13), express T and U in terms of our integrations variables $\hat{s}$, t, $\hat{t}$, φ^* and we have used them to relate the lab frame variables to the integration ones, as shown in the next appendix.

APPENDIX B: KINEMATICS IN THE LAB FRAME (ELASTIC)

In this appendix, we give the kinematics of the same process in the lab frame. The 4 momenta of the particles are given by:

incident electron: $l \equiv (E_e,\, 0,\, 0,\, -E_e)$,

incident proton: $P \equiv (E_p,\, 0,\, 0,\, P_p)$, where $P_p^* = \sqrt{{E_p}^2 - m^2}$,

outgoing electron: $l' \equiv E'_e(1,\, \sin\theta_e,\, 0,\, \cos\theta_e)$,

outgoing photon: $k' \equiv E'_\gamma(1,\, \sin\theta_\gamma\cos\phi_\gamma,\, \sin\theta_\gamma\sin\phi_\gamma,\, \cos\theta_\gamma)$.

Here we have chosen the frame such that the outgoing electron has zero azimuthal angle. The Lorentz invariants are:

$$\hat{s} = (l' + k')^2 = 2E'_e E'_\gamma(1 - \sin\theta_e\sin\theta_\gamma\cos\phi_\gamma - \cos\theta_e\cos\theta_\gamma), \tag{B1}$$

$$\hat{t} = (l - l')^2 = -2E_e E'_e(1 + \cos\theta_e), \tag{B2}$$

$$\hat{u} = (l - k')^2 = -2E_e E'_\gamma(1 + \cos\theta_\gamma), \tag{B3}$$

$$S = (l+P)^2 = m^2 + 2E_e(E_p + P_p), \tag{B4}$$

$$T = (P-l')^2 = m^2 - 2E'_e(E_p - P_p\cos\theta_e), \tag{B5}$$

$$U = (P-k')^2 = m^2 - 2E'_\gamma(E_p - P_p\cos\theta_\gamma). \tag{B6}$$

The polar angles in the lab frame can be written in terms of the invariants and the incident energies:

$$\cos\theta_e = \frac{E_p\ \hat{t} - E_e\ (T-m^2)}{P_p\ \hat{t} + E_e\ (T-m^2)}, \tag{B7}$$

$$\cos\theta_\gamma = \frac{E_p\ (t-\hat{s}-\hat{t}) - E_e\ (U-m^2)}{P_p\ (t-\hat{s}-\hat{t}) + E_e\ (U-m^2)}. \tag{B8}$$

In the same way, for the energies of the final electron and photon we have:

$$E'_e = -\frac{\hat{t}\ P_p + E_e\ (T-m^2)}{S-m^2}, \tag{B9}$$

$$E'_\gamma = \frac{P_p\ (\hat{s}-t+\hat{t}) - E_e\ (U-m^2)}{S-m^2}. \tag{B10}$$

The azimuthal angle of the outgoing photon is:

$$\cos\phi_\gamma = \frac{2E'_eE'_\gamma(1-\cos\theta_e\cos\theta_\gamma) - \hat{s}}{2E'_eE'_\gamma\sin\theta_e\sin\theta_\gamma}, \tag{B11}$$

which is related to the acoplanarity angle by the relation $\phi = |\,\pi - \phi_\gamma\,|$. Using Eqs. (A7) and (A8) together with Eqs. (A11)-(A13), the formulae above for $\cos\theta_e$, $\cos\theta_\gamma$, E'_e , E'_γ and $\cos\phi_\gamma$ can be expressed in terms of the invariants and the incident energies. Eqs. (B7)-(B11) are needed to implement numerically the kinematical region under study, since they relate the lab variables (energies and angles) to the ones used for the integration.

APPENDIX C: KINEMATICS IN THE $e-\gamma$ C. M. FRAME (INELASTIC)

In this frame most of the expressions remain the same as given in appendix A. The relations among the invariants are now:

$$\hat{s} + \hat{t} + \hat{u} = -Q^2, \qquad S + T + U = 3m^2 + \frac{Q^2}{x_B}, \tag{C1}$$

where $Q^2 = -t$ and x_B can be written as

$$x_B = \frac{Q^2}{Q^2 + W^2 - m^2}. \tag{C2}$$

The only formulae which are different are the ones involving E_p^* and $\cos\theta_p^*$. So Eq. (A11) will be replaced by

$$E_p^* = \frac{S - Q^2 - W^2}{2\sqrt{\hat{s}}}, \qquad P_p^* = \frac{\sqrt{(S - Q^2 - W^2)^2 - 4\hat{s}m^2}}{2\sqrt{\hat{s}}}, \qquad E'^* = \frac{\sqrt{\hat{s}}}{2}, \tag{C3}$$

while for the angles:

$$\cos\theta^* = -\frac{Q^2 + \hat{s} + 2\hat{t}}{\hat{s} + Q^2}, \tag{C4}$$

and

$$\cos\theta_p^* = \frac{2\hat{s}\,(S - m^2) - (S - Q^2 - W^2)(\hat{s} + Q^2)}{(\hat{s} + Q^2)[(S - Q^2 - W^2)^2 - 4\hat{s}m^2]^{\frac{1}{2}}}. \tag{C5}$$

Eqs. (C3)-(C5) reduce to the Eqs. (A11)-(A13) of the elastic channel for $W = m$ and $Q^2 = -t$.

APPENDIX D: KINEMATICS IN THE LAB FRAME (INELASTIC)

The invariants in the case of inelastic scattering are the same as in the elastic case: Eqs. (B1)-(B6). Eq. (C1) describes the relation among them. The expressions of $\cos\theta_e$, $\cos\theta_\gamma$, E'_e, E'_γ and $\cos\phi_\gamma$, in terms of the integration variables W^2, $\hat{s}$, Q^2, $\hat{t}$, φ^* are given by Eqs. (B7)-(B11) together with Eqs. (A7), (A8) as before, but now Eqs. (C3)-(C5) will replace Eqs. (A11)-(A13).

---

[1] C.F. Weizsäcker, Z. Phys. **88**, 612 (1934); E. J. Williams, Phys. Rev. **45**, 729 7(L), (1934).

[2] B. Kniehl, Phys. Lett. **B 254**, 267, (1991).

[3] M. Drees, R. M. Godbole, M. Nowakowski, S. Rindani, Phys. Rev. **D 50**, 2335 (1994).

[4] J. Ohnemus, T. F. Walsh, P. M. Zerwas, Phys. Lett. **B 328**, 369 (1994).

[5] M. Glück, M. Stratmann, W. Vogelsang, Phys. Lett. **B 343**, 399 (1995).

[6] A. De Rujula, W. Vogelsang, Phys. Lett. **B 451** 437 (1999).

[7] M. Glück, C. Pisano, E. Reya, Phys. Lett. **B 540**, 75, (2002).

[8] M. Glück, C. Pisano, E. Reya, I. Schienbein, Eur. Phy. J. **C 27**, 427 (2003).

[9] V. Lenderman, Ph. D. thesis, Univ. Dortmund, H1 collaboration, DESY-THESIS-2002-004, (2002).

[10] A. Courau and P. Kessler, Phys. Rev. **D 46**, 117, (1992).

[11] J. Blümlein, G. Levman, H. Spiesberger, J. Phys. **G 19**, 1695 (1993).

[12] C. G. Callan and D. J. Gross, Phys. Rev. Lett. **22**, 156 (1969).

[13] A. Courau, HERA Note H1-187 (unpublished); A. Courau, S. Kermiche, T. Carli, P. Kessler, HERA Note H1-207 (unpublished).

[14] X. Ji, Phys. Rev. **D 55**, 7114 (1997).

[15] H. Anlauf, Habilitation thesis, Seigen Univ., hep-ph/0211456.

[16] H. Abramowicz and A. Levy, hep-ph/9712415.

[17] H. Anlauf, H. D. Dahmen, P. Manakos,, T. Mannel, T. Ohl, Comput. Phys. Commun. **70**,97 (1992).

[18] M. Glück, E. Reya, A. Vogt, Eur. Phys. J. **C 5**, 461 (1998).

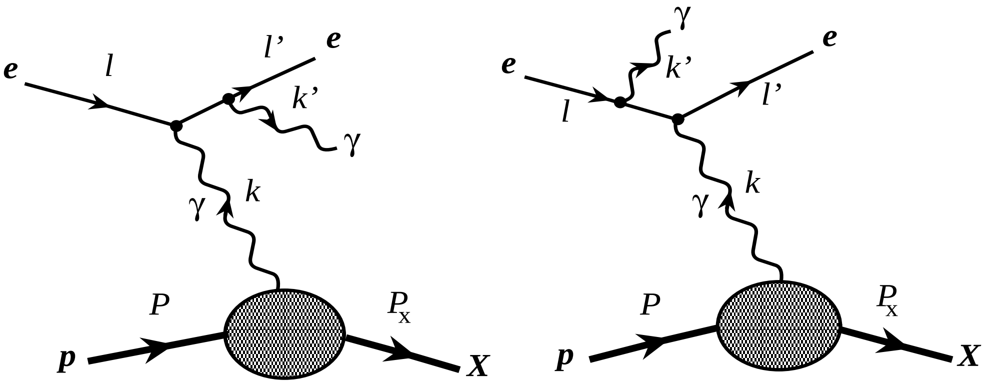

Fig. 1: Feynman diagrams considered for $ep \rightarrow e\gamma X$, with a real final state photon ($k'^2 = 0$).

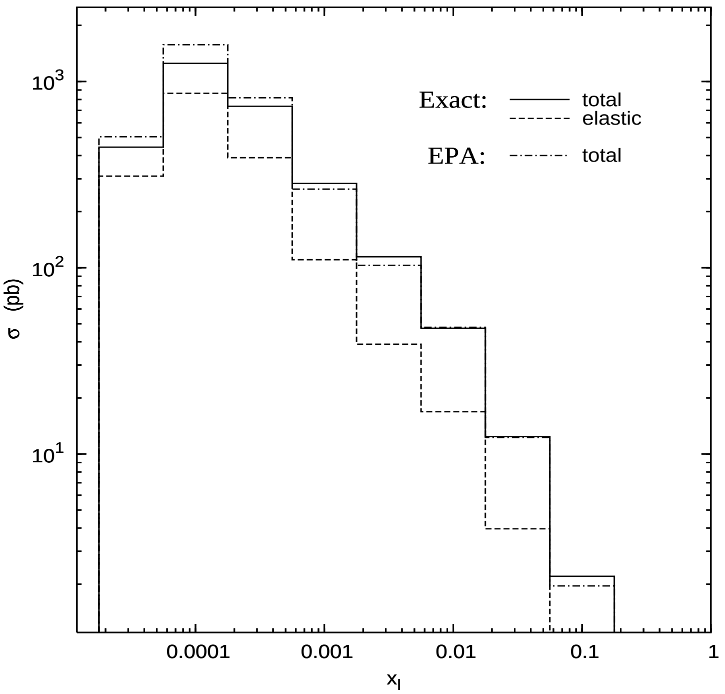

Fig. 2: Cross section for Compton process at HERA-H1. The cuts applied are as described in the text.

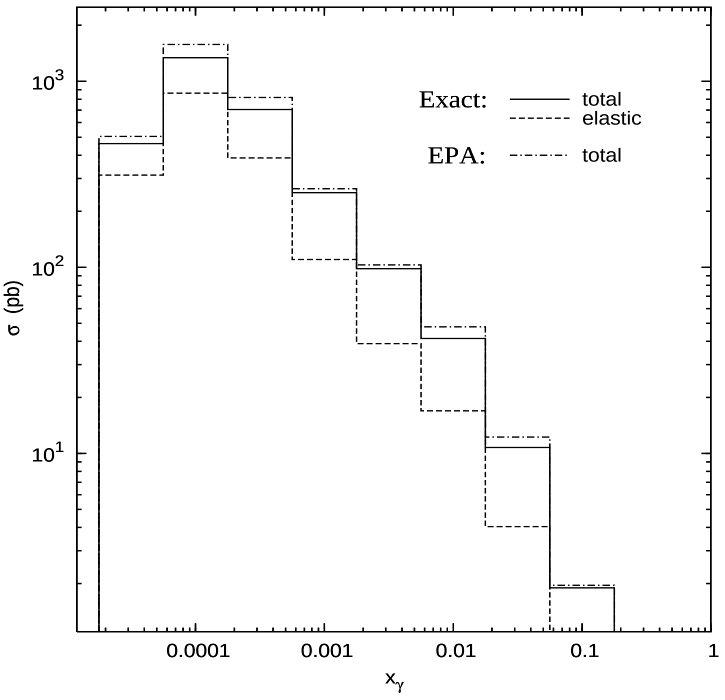

Fig. 3: Cross section for Compton process at HERA-H1. The bins are in x_γ. The cuts applied are as described in the text.

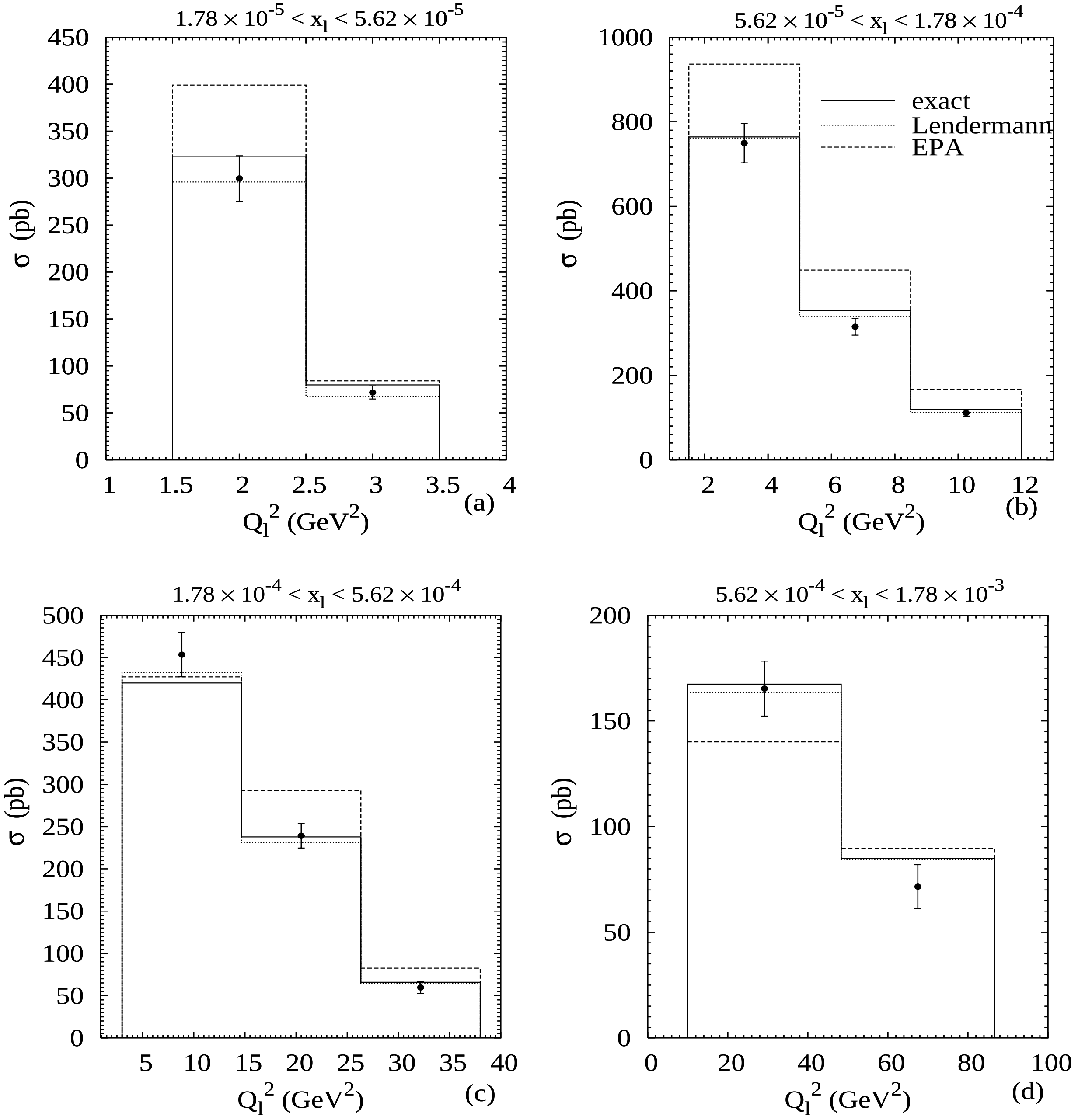

Fig. 4: Double differential cross section for QED Compton scattering at HERA-H1. The data are taken from [9]. The kinematical bins correspond to Table 1. The continuous line corresponds to our exact calculation, the dotted line to the calculation in [9] and the dashed line to the EPA.

x bin	Q_l^2 bin	σ_{el}	$\sigma_{\mathrm{el}}^{\mathrm{Len}}$	σ_{el}^{*}	$\sigma_{\mathrm{el}}^{\mathrm{EPA}}$
$1.78 \times 10^{-5} - 5.62 \times 10^{-5}$	$1.5 - 2.5$	2.428×10^{2}	2.342×10^{2}	2.446×10^{2}	2.461×10^{2}
$1.78 \times 10^{-5} - 5.62 \times 10^{-5}$	$2.5 - 3.5$	5.099×10^{1}	4.71×10^{1}	5.201×10^{1}	5.051×10^{1}
$5.62 \times 10^{-5} - 1.78 \times 10^{-4}$	$1.5 - 5.0$	5.279×10^{2}	5.319×10^{2}	5.259×10^{2}	5.247×10^{2}
$5.62 \times 10^{-5} - 1.78 \times 10^{-4}$	$5.0 - 8.5$	2.396×10^{2}	2.327×10^{2}	2.404×10^{2}	2.395×10^{2}
$5.62 \times 10^{-5} - 1.78 \times 10^{-4}$	$8.5 - 12.0$	8.496×10^{1}	8.32×10^{1}	8.559×10^{1}	8.571×10^{1}
$1.78 \times 10^{-4} - 5.62 \times 10^{-4}$	$3.0 - 14.67$	2.080×10^{2}	2.036×10^{2}	2.056×10^{2}	2.061×10^{2}
$1.78 \times 10^{-4} - 5.62 \times 10^{-4}$	$14.67 - 26.33$	1.373×10^{2}	1.388×10^{2}	1.373×10^{2}	1.372×10^{2}
$1.78 \times 10^{-4} - 5.62 \times 10^{-4}$	$26.33 - 38.0$	3.712×10^{1}	3.86×10^{1}	3.720×10^{1}	3.695×10^{1}
$5.62 \times 10^{-4} - 1.78 \times 10^{-3}$	$10.0 - 48.33$	5.947×10^{1}	5.71×10^{1}	5.918×10^{1}	5.921×10^{1}
$5.62 \times 10^{-4} - 1.78 \times 10^{-3}$	$48.33 - 86.67$	3.714×10^{1}	3.85×10^{1}	3.715×10^{1}	3.704×10^{1}
$5.62 \times 10^{-4} - 1.78 \times 10^{-3}$	$86.67 - 125.0$	1.056×10^{1}	1.028×10^{1}	1.057×10^{1}	1.054×10^{1}
$1.78 \times 10^{-3} - 5.62 \times 10^{-3}$	$22 - 168$	1.913×10^{1}	1.877×10^{1}	1.909×10^{1}	1.909×10^{1}
$1.78 \times 10^{-3} - 5.62 \times 10^{-3}$	$168 - 314$	1.239×10^{1}	1.229×10^{1}	1.239×10^{1}	1.238×10^{1}
$1.78 \times 10^{-3} - 5.62 \times 10^{-3}$	$314 - 460$	5.917	6.02	5.915	5.914
$5.62 \times 10^{-3} - 1.78 \times 10^{-2}$	$0 - 500$	4.811	5.76	4.890	4.890
$5.62 \times 10^{-3} - 1.78 \times 10^{-2}$	$500 - 1000$	9.271	9.22	9.264	9.271
$5.62 \times 10^{-3} - 1.78 \times 10^{-2}$	$1000 - 1500$	2.572	2.65	2.571	2.573
$1.78 \times 10^{-2} - 5.62 \times 10^{-2}$	$0 - 1500$	8.238×10^{-1}	6.8×10^{-1}	9.085×10^{-1}	9.086×10^{-1}
$1.78 \times 10^{-2} - 5.62 \times 10^{-2}$	$1500 - 3000$	2.431	2.69	2.430	2.434
$1.78 \times 10^{-2} - 5.62 \times 10^{-2}$	$3000 - 4500$	6.336×10^{-1}	7.7×10^{-1}	6.328×10^{-1}	6.345×10^{-1}
$5.62 \times 10^{-2} - 1.78 \times 10^{-1}$	$10 - 6005$	3.120×10^{-1}	4.27×10^{-1}	3.120×10^{-1}	3.117×10^{-1}
$5.62 \times 10^{-2} - 1.78 \times 10^{-1}$	$6005 - 12000$	2.437×10^{-1}	2.13×10^{-1}	2.438×10^{-1}	2.436×10^{-1}
$5.62 \times 10^{-2} - 1.78 \times 10^{-1}$	$12000 - 17995$	0.000	0.000	0.000	2.461×10^{-2}

TABLE I: Double differential (elastic) QED Compton scattering cross section. σ_{el} is the exact result in Eq. (2.23), $\sigma_{\mathrm{el}}^{\mathrm{Len}}$ corresponds to the results in [9]. The x-bins refer to x_l in Eq. (2.34) except for σ_{el}^{*} where they refer to x_γ in Eq. (2.33). $\sigma_{\mathrm{el}}^{\mathrm{EPA}}$ is given in Eq. (2.28) where $x \equiv x_\gamma$. Q_l^2 is expressed in GeV^2 and the cross-sections are in pb.

x bin	Q_l^2 bin	$\sigma_{\rm inel}$	$\sigma_{\rm inel}^{\rm Len}$	$\sigma_{\rm inel}^{*}$	$\sigma_{\rm inel}^{\rm EPA}$
$1.78 \times 10^{-5} - 5.62 \times 10^{-5}$	$1.5 - 2.5$	7.996×10^{1}	6.170×10^{1}	7.503×10^{1}	1.529×10^{2}
$1.78 \times 10^{-5} - 5.62 \times 10^{-5}$	$2.5 - 3.5$	2.880×10^{1}	2.050×10^{1}	4.142×10^{1}	3.361×10^{1}
$5.62 \times 10^{-5} - 1.78 \times 10^{-4}$	$1.5 - 5.0$	2.361×10^{2}	2.296×10^{2}	2.364×10^{2}	4.116×10^{2}
$5.62 \times 10^{-5} - 1.78 \times 10^{-4}$	$5.0 - 8.5$	1.139×10^{2}	1.062×10^{2}	1.500×10^{2}	2.099×10^{2}
$5.62 \times 10^{-5} - 1.78 \times 10^{-4}$	$8.5 - 12.0$	3.442×10^{1}	2.890×10^{1}	6.291×10^{1}	8.094×10^{1}
$1.78 \times 10^{-4} - 5.62 \times 10^{-4}$	$3.0 - 14.67$	2.119×10^{2}	2.287×10^{2}	1.278×10^{2}	2.210×10^{2}
$1.78 \times 10^{-4} - 5.62 \times 10^{-4}$	$14.67 - 26.33$	1.005×10^{2}	9.230×10^{1}	1.220×10^{2}	1.556×10^{2}
$1.78 \times 10^{-4} - 5.62 \times 10^{-4}$	$26.33 - 38.0$	2.868×10^{1}	2.570×10^{1}	4.682×10^{1}	4.558×10^{1}
$5.62 \times 10^{-4} - 1.78 \times 10^{-3}$	$10.0 - 48.33$	1.079×10^{2}	1.064×10^{2}	5.383×10^{1}	8.092×10^{1}
$5.62 \times 10^{-4} - 1.78 \times 10^{-3}$	$48.33 - 86.67$	4.779×10^{1}	4.590×10^{1}	5.690×10^{1}	5.272×10^{1}
$5.62 \times 10^{-4} - 1.78 \times 10^{-3}$	$86.67 - 125.0$	1.315×10^{1}	1.132×10^{1}	2.050×10^{1}	1.587×10^{1}
$1.78 \times 10^{-3} - 5.62 \times 10^{-3}$	$22 - 168$	4.758×10^{1}	4.917×10^{1}	2.426×10^{1}	3.080×10^{1}
$1.78 \times 10^{-3} - 5.62 \times 10^{-3}$	$168 - 314$	2.010×10^{1}	1.735×10^{1}	2.350×10^{1}	2.058×10^{1}
$1.78 \times 10^{-3} - 5.62 \times 10^{-3}$	$314 - 460$	6.940	5.760	9.303	1.021×10^{1}
$5.62 \times 10^{-3} - 1.78 \times 10^{-2}$	$0 - 500$	1.482×10^{1}	1.432×10^{1}	7.327	8.825
$5.62 \times 10^{-3} - 1.78 \times 10^{-2}$	$500 - 1000$	1.228×10^{1}	9.890	1.318×10^{1}	1.687×10^{1}
$5.62 \times 10^{-3} - 1.78 \times 10^{-2}$	$1000 - 1500$	3.135	2.600	3.756	4.885
$1.78 \times 10^{-2} - 5.62 \times 10^{-2}$	$0 - 1500$	3.585	2.500	1.623	1.811
$1.78 \times 10^{-2} - 5.62 \times 10^{-2}$	$1500 - 3000$	3.778	2.150	3.866	4.867
$1.78 \times 10^{-2} - 5.62 \times 10^{-2}$	$3000 - 4500$	9.675×10^{-1}	6.600×10^{-1}	1.088	1.341
$5.62 \times 10^{-2} - 1.78 \times 10^{-1}$	$10 - 6005$	1.093	1.460×10^{-1}	6.589×10^{-1}	7.147×10^{-1}
$5.62 \times 10^{-2} - 1.78 \times 10^{-1}$	$6005 - 12000$	5.496×10^{-1}	2.110×10^{-1}	5.782×10^{-1}	5.922×10^{-1}
$5.62 \times 10^{-2} - 1.78 \times 10^{-1}$	$12000 - 17995$	6.164×10^{-2}	4.300×10^{-2}	0.000	6.791×10^{-2}

TABLE II: Double differential (inelastic) QED Compton scattering cross section. $\sigma_{\rm inel}$ is the exact result in Eq. (3.10), $\sigma_{\rm inel}^{\rm Len}$ corresponds to the results in [9]. The x-bins are as in Table I, *i.e.* refer to x_l in Eq. (2.34) except for $\sigma_{\rm inel}^{*}$ where they refer to x_γ in Eq. (2.33). $\sigma_{\rm inel}^{\rm EPA}$ is given in Eq. (3.13) where $x \equiv x_\gamma$. Q_l^2 is expressed in GeV^2 and the cross-sections are in pb.